NUKLEONIKA 2016;61(2):119–124
doi: 10.1515/nuka-2016-0021

ORIGINAL PAPER

DE GRUYTER
OPEN

# Ambient fields generated by a laser spark

**Karel Rohlena,**
**Martin Mašek**

**Abstract.** The electric and magnetic fields surrounding a laser spark formed after an optical breakdown due to a focused nanosecond laser beam in a gaseous environment are examined in order to assess their possible influence on the processes going on in the gas medium, mainly chemical reactions triggered by the spark plasma radiation. The magnetic field is generated by the standard mechanism of crossed electron density and temperature gradients, the electric field is supposed to be produced by the plasma polarization due to its radial expansion across the self-generated magnetic field. A simple model of spark plasma formation near the tip of the focal cone is assumed, with a delayed breakdown, which allows the focused laser light to sweep the whole volume of the forming spark right down to the focal caustic and thus to form a centimeter long plasma cone. In this conical geometry, the value of plasma electric dipole moment is evaluated as a measurable quantity as well as approximate values of the electric and magnetic field near the focal caustic, where they both tend to grow in magnitude.

**Key words:** laser spark • radiation chemistry • field generation

K. Rohlena✉, M. Mašek
Institute of Physics ASCR (Fyzikální ústav AVČR),
Na Slovance 2, 182 21 Prague 8 – Libeň,
Czech Republic,
Tel.: +420 266 052 792, Fax: +420 286 890 265,
E-mail: rohlena@fzu.cz

Received: 25 September 2015
Accepted: 4 December 2015

## Introduction

An optical breakdown caused by a nanosecond laser beam focused into a gaseous medium forms a laser spark in the given gaseous environment. The most likely processes triggered by the spark are those of radiation chemistry forming radicals and more complex molecules from originally simple gas components. Owing to its high energy density, the laser spark is an ideal instrument to simulate the energetic events in the planetary atmospheres, such as meteorite impacts. The spark, however, generates not only the radiation, but also ambient macroscopic electric and magnetic fields, which may influence the outcome of the mentioned radiation synthesis. The most striking example is sometimes the absence racemization of optically active products (enantiomeric imbalance), i.e. a surplus of one kind of optical isomer. This concerns molecules like amino acids [1, 2], which are thought later to have participated in more complex organic syntheses leading to the origin of terrestrial life. A useful survey on laser plasma chemistry is to be found in [3]. Quite recently, experiments involving heterogeneous systems with the liquid formamide as a primitive compound have been arranged in a similar configuration and it was found that all the four nucleobase constituents of RNA can be synthesized by a single laser shot, as shown in [4]. As mentioned above, some of the created molecules

may be optically active and it has been established as an experimental fact that the model experiments in the gas-filled chamber yield an uneven ratio of right-hand (R-) and left-hand (L-) optical isomers. It has been conjectured (see e.g. [5]) that this asymmetry between the R- and L-species is induced by a synthesis going on under the action of superimposed electric and magnetic fields occurring in the spark vicinity, as a consequence of its polarization and internal currents. Such fields during an optical breakdown in the air have actually been directly measured, as shown in [6]. The orientation of the electric dipole formed in the plasma, which is caused by the polarization due to the plasma radial expansion in the self-generated magnetic field, has the polarity, which very much depends on the disposition of electron density and electron temperature gradients inside the plasma. These gradients depend, in turn, on the mechanism of the laser spark formation. In the literature, essentially three different mechanisms can be tracked down: (1) a light detonation wave described in [7], (2) the radiation hydrodynamics supersonic propagation, as considered in [8], and (3) a delayed breakdown action relevant for a tapering geometry of the beam, also described in [7]. The present contribution is aiming at an assessment of the mentioned spark formation models and their comparison with the experimental findings.

## Mechanism of the laser spark

The laser spark in a gas at the atmospheric pressure is initiated by an optical breakdown in the gas into which a high power laser beam is focused. The optical discharge starts inside the focal cone in the place where the focused intensity attains the breakdown value characteristic of the gas mixture and its pressure. The propagation of the ionization front from the breakdown point, due to which the laser spark is formed may occur in three different regimes in dependence on the duration, focusing and intensity of the driving laser pulse. They are described in [7]. For long pulses, the most fundamental mechanism is the 'light detonation wave' with the characteristic velocity $D \sim (I_L/h)^{1/3}$ of propagation against the laser beam (see [7], where $I_L$ is the local laser beam intensity and $h$ is the initial mass density of the ambient gas.

The speed of the plasma front may reach 100 km/s, but it is not enough for short pulses to form large spark plasma, as it is observed experimentally. The propagation may still be enhanced by the second mechanism of supersonic radiative wave propagation driven by X-ray radiation emanating from the forming plasma in both the longitudinal and the radial directions (see [8]), but even this mechanism needs a longer time of several nanoseconds to form a sizable plasma. For very short pulses, as produced by the sub-nanosecond iodine laser and plasma formed within a focused tapering beam, the most likely mechanism seems to be the delayed breakdown action equally described in [7].

A short pulse with a steep leading edge easily reaches the steady-state intensity breakdown value somewhere on its way down the focal cone, but before the actual breakdown occurs (since it takes some time for the necessary electron avalanche to develop), the front end of the pulse moves farther on still closer to the focus undisturbed by any plasma effects. When the intensity keeps rising up, the initial breakdown eventually takes place closer to the focus than given by the nominal CW breakdown intensity and the resulting breakdown front travels very fast against the laser beam to the point where the nominal breakdown intensity was first reached. The mechanism of the delay consists in only a gradual build up of the pre-breakdown avalanche and the actual breakdown occurs only if a limiting electron density within the avalanche is reached, which takes a certain time to build up. If the rate of the electron multiplication is supposed to be proportional to the local power density, the speed of the breakdown front is in this case proportional to $\sim I_L^{1/2}$. This is the reason why for intense nanosecond laser pulses in a tapering geometry the propagation velocity of the breakdown wave must, in principle, be faster than the light detonation wave velocity, see e.g. [7]. In this way, a large plasma formation is created in the form of a truncated cone with the narrow side facing the focus, as shown in Fig. 1.

It is a remarkable property of this initial plasma formation that the plasma density is rising up from the focal side toward the laser, with a sharp drop in the density on the laser side. The critical density for the iodine laser wavelength $\lambda = 1.3$ μm is about $6.4 \times 10^{20}$ cm$^{-3}$, which is more than at the atmospheric pressure all the mixture components taken together can contribute in terms of free electrons even if fully ionized, so that no critical surface can be formed within the plasma and the beam could, in principle, continue to propagate down the focal cone. However, after the plasma is formed, the propagating beam will be defocused and scattered by the resulting refraction index inhomogeneities,

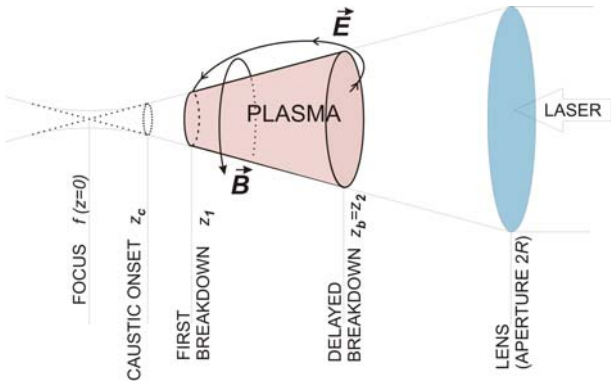


**Fig. 1.** Scheme of the laser spark plasma immediately after the breakdown. The plasma is supposed to have a form of truncated cone limited by the delayed nominal breakdown surface on the laser side ($z_1 = z_b$) and the actual first breakdown ($z_1 \to z_c$) facing the focus. The reference frame uses the optical axis oriented against the laser beam as the $z$-axis ($z = 0$ at the ideal focus) and the positive azimuthal direction is anticlockwise. The field lines of both the electric $\vec{E}$ and magnetic $\vec{B}$ fields are schematically shown.

thus blocking any further plasma creation on the focal side of the spark.

## Electric and magnetic fields around the laser spark

The laser spark is an energetic phenomenon capable of forming electric and magnetic fields in its vicinity. Here we shall be interested primarily in the evaluation of the fields generated by the spark in its active stage or shortly after. We shall thus consider a plasma cloud in the form of tapered truncated cone partially filling the focal cone with the geometrical focus placed in the origin of coordinates and the laser light propagating against the $z$-axis. The mechanism creating an azimuthal magnetic field winding round the spark plasma is well known. Its generation equation is derived by $\vec{B} = (0, B_\varphi, 0)$ combining the electron equation of motion with the electron inertia neglected, Faraday's law and the Ampère's law of the Maxwell's equations.

$$\frac{\partial \vec{B}}{\partial t} - \mathrm{rot}\left[\vec{v} \times \vec{B}\right] - \frac{c^2}{4\pi\sigma_E}\Delta\vec{B} + \mathrm{rot}\left[\frac{\vec{j}}{en_e} \times \vec{B}\right] = c\ \mathrm{rot}\left(\frac{\mathrm{grad}\, p_e}{en_e}\right) \tag{1}$$

Keeping the source term only (i.e., dropping the convective, diffusive, and Hall terms on the left-hand side), the following equation is obtained:

$$\frac{\partial \vec{B}}{\partial t} = \frac{ck_B}{en}\left[\mathrm{grad}\, T \times \mathrm{grad}\, n\right] \tag{2}$$

where $e$ is the elementary charge, $c$ the speed of light, $k_B$ the Boltzmann constant, $n$ the electron number density, $T$ the electron temperature, and $\sigma_E$ the plasma electric conductivity. In the following text, cylindrical coordinates $(r, \varphi, z)$ will be used with the zero in the ideal focus, the optical $z$-axis oriented against the laser beam and the positive direction of $\varphi$ in the anticlockwise sense. The solution of Eq. (2) can be found in model cases, but for our purposes, it is sufficient to take an approximation. However, in contrast to the case of a solid target, the density gradient in the case of the laser spark is rising away from the breakdown point toward the laser (positive $z$-axis direction). The field has, thus in the case of mostly flatter dependence of the electron temperature along the $z$-axis, still a purely azimuthal direction but it winds round the beam direction in the anticlockwise sense, and its only non-vanishing component $B_\varphi$ is thus positive. Modelling of the radial dependence of density and temperature is done with simple parabolas, respecting simultaneously the focal cone tapering

$$\begin{aligned} n(r,z) &= n_0\left(1 - \left(\frac{rf}{Rz}\right)^2\right) P_n\left(z / z_n\right) \\ T(r,z) &= T_0\left(1 - \left(\frac{rf}{Rz}\right)^2\right) P_T\left(z / z_T\right) \end{aligned} \tag{3}$$

where $f$ is the focal distance and $R$ is the aperture radius, $n_0$ and $T_0$ are density and temperature values on the optical axis in the caustic region ($n_0$ cancels out), and $P_n(z/z_n)$ as well as $P_T$ $(z/z_T)$ are so far unspecified longitudinal profile functions of density and temperature in the $z$-direction, governed by the scale lengths $z_n$ and $z_T$, respectively. A simple estimate renders

$$B_\varphi \doteq \frac{2c}{e} k_B T_0 \tau_L r \left(\frac{f}{zR}\right)^2 \left(\frac{P_n' P_T}{z_n P_n} - \frac{P_T'}{z_T}\right) \tag{4}$$

where $\tau_L$ is the laser pulse duration and the primes at the profile functions $P_n$ and $P_T$ designate the derivatives with respect to their arguments. It should be noted that with a rising density profile ($P_n' > 0$) the magnetic field is now winding round the spark channel in the opposite sense than in the conventional laser experiments involving solid targets. For identical longitudinal density and temperature profiles $P_n(z/z_n) = P_T(z/z_T)$ and $z_n = z_T$ (implying colinearity), the field turns to be zero. The magnetic field near the surface of the plasma cone forming the spark is given by

$$B_\varphi \doteq \frac{2c}{e} k_B T_0 \tau_L \frac{f}{zR}\left(\frac{P_n' P_T}{z_n P_n} - \frac{P_T'}{z_T}\right) \tag{5}$$

which means that although on the laser side where the local cone cross-section is relatively large, the resulting magnetic field might be weak, in the direction to the focus $z \to 0$, the field intensity is growing and would reach infinity at an ideal point-like focus. In reality, of course, the field growth is confined by the finite radius $r_c$ of the focal caustic at the point $z_c = r_c f/R$. The local magnetic field intensity near the plasma cone tip may thus reach quite a high value $B(z_c) \sim (z_b/z_c)B(z_b)$, where $z_b$ is the point of the delayed breakdown on the laser side $z_b = r_b f/R$ (the broader end of the plasma cone facing the laser with the radius $r_b$ is derivable from the nominal value of the laser breakdown intensity, for details see [7], p. 176). Since the first breakdown takes place on the focal (narrow) side of the focal cone, there is some time left for the plasma on this side to diffuse laterally, by which this part of the cone is expanded and the tapering angle is reduced. The local plasma expansion near the tip is, obviously, accelerated by the presence of the sharp gradients. Simultaneously, this expansion means also a rarefaction of the plasma starting at the cone tip, by which the positive longitudinal density gradient is gradually formed, as shown in [7].

As regards the origin of the electric field, it was conjectured in paper [6] that streaming of the expanding plasma across the magnetic field is causing a charge separation (polarization), inducing for an ideally conducting plasma a charge density $\rho$ and a longitudinal electric $\vec{d} = (0, 0, d_z)$ dipole moment of the spark

$$\begin{aligned} \rho &= -\frac{1}{4\pi c} div\left(\left[\vec{v} \times \vec{B}\right]\right) \\ &= -\frac{k_B T_0 \tau_L}{2\pi} r v_r \frac{d}{dz}\left[\left(\frac{f}{Rz}\right)^2 \left(\frac{P_n' P_T}{z_n P_n} - \frac{P_T'}{z_T}\right)\right] \end{aligned} \tag{6}$$

where $\rho$ is the charge density, and $\vec{v} = (v_r, 0, v_z)$ is the plasma flow velocity mainly in the radial direction. In the following, we shall approximate its value by

(a constant) acoustic speed equal to $v_r \sim \sqrt{k_B T_0/m_i}$; $m_i$ is the weighted ion mass. This introduces a certain inconsistency, since the spark is initially confined by the cold surrounding gas, which blocks any convective plasma expansion, and also the true $v_r$ should vanish on the optical axis for symmetry reasons. However, a more realistic approximation of $v_r$ just complicates the model and leads to changes in numerical coefficients in the resulting expressions only. A plasma expansion may, however, proceed by the diffusion. For the dipole moment of the spark $d_z$ it is thus obtained

$$(7)\quad d_z = \int d\vec{r}' z\rho = -\frac{1}{3}\frac{(k_B T_0)^{3/2}}{e\sqrt{m_i}} \cdot \tau_L \frac{R}{f}\int_{z_1}^{z_2} dz\, z^4 \frac{d}{dz}\left[\frac{1}{z^2}\left(\frac{P_n' P_T}{z_n P_n} - \frac{P_T'}{z_T}\right)\right] = \frac{(k_B T_0)^{3/2}}{e\sqrt{m_i}} \tau_L \frac{R}{f} \cdot z_b \begin{cases} 1/3 \text{ (exponential)} \\ \nu(3/2 - 2\log 2) \sim 0.114\nu \text{ (power } \nu) \end{cases}$$

The last line is corresponding to the case of a flat temperature profile in the $z$-direction, $P_T(z/z_T) = 1$ and to an exponential $P_n(z/z_n) \sim \exp(z/z_n)$ or a power dependence $P_n(z/z_n) \sim (z/z_n + 1)^\nu$ (including linear $\nu = 1$ or quadratic $\nu = 2$ cases, the shift by 1 has been added to avoid a nonphysical zero in the density dependence as $z \to 0$, which would introduce spurious singularities when approaching the focus). The density profile is actually changing with time, which in our model might be expressed with a time dependent density scale-length $z_n$. An idea about the density profile across the laser spark and its temporal evolution can be obtained by inspecting Fig. 6.8 on p. 172 in Ref. [7]. There is no similar information available for the temperature profile, however, it can be expected that owing to the diminishing intensity of the beam and growth of the heated plasma volume when going away from the tip, the temperature might be falling ($P_T' < 0$) adding thus to the rising density effect. For the purpose of our calculation, however, we set $P_T = 1$, eliminating the temperature profile contribution. Since the plasma assumes the shape of the truncated cone, the integration limits $z_1$ and $z_2$ are given as the points of the first actual breakdown on the focal side ($z_1$) and of the delayed nominal breakdown ($z_2 = z_b$) on the laser side. Naturally, the actual breakdown can well take place still before the laser pulse reaches the caustic, but the caustic is at any rate the utmost point where the first breakdown might occur at all. The density scale length $z_n$, which is (in principle) time dependent, was also set equal to $z_b$ and where possible $z_1$ will be replaced either by the $z_c$ coordinate of the onset of focal caustic ($z_c = r_c f/R$, where $r_c$ is the caustic radius), or even by the ideal focus ($z_1 = 0$), as it was the case of the above dipole moment integral. The dipole moment has the correct positive orientation along the $z$-axis (positive charge nearer to the laser), as indeed was found experimentally [6].

## Electric field near the focal cone caustic

The value of the electric dipole set-up by the plasma cone, though a directly measurable quantity does not characterize the electric field intensity near the cone tip with a sufficient accuracy, since the dipole approximation is valid at a larger distance from the field source only. A more detailed estimate is therefore needed to obtain a realistic field value near the tip. We shall start from the general relation for the field potential

$$(8)\qquad \varphi(\vec{r}) = \int d\vec{r}' \frac{\rho(\vec{r}')}{|\vec{r} - \vec{r}'|}$$

where $\rho$ is the spark charge density given by Eq. (6). Owing to the axial symmetry, the integration can be again performed in cylindrical coordinates, giving in the first step (angular integration)

$$(9)\quad \varphi(r,z) = \int_{z_1}^{z_2} dz' \int_0^{Rz'/f} dr' r' \rho(r',z') \left[ \frac{K\left(\frac{4rr'}{(r+r')^2 + (z-z')^2}\right)}{\sqrt{(r+r')^2 + (z-z')^2}} + \frac{K\left(\frac{4rr'}{(r-r')^2 + (z-z')^2}\right)}{\sqrt{(r-r')^2 + (z-z')^2}} \right]$$

where in the cylindrical geometry $r = |\vec{r}_\perp|$ means the perpendicular radius, and $|z| = |\vec{r}_\parallel|$ is the distance from the focus along the optical axis (same for the primed variables), $z_1$, $z_2$ are again the integration limits in the focal direction as explained in the case of the electric dipole integral. $K(\kappa) \approx \pi/2\ (1 + \kappa^2/4 + 9\kappa^4/64 + \ldots)$ is the elliptic integral of the first kind. Since we are mainly interested in the field near the tip $r << R$, $z << f$, it is meaningful to expand Eq. (9) in the coordinates $r$, $z$. The absolute term in the potential can be dropped and the linear terms will give an approximation of the field components at the tip. An analysis of Eq. (9) shows that the linear term in $r$ vanishes (as it, indeed, has to vanish for the symmetry reasons), and the following quadratic term thus contributes little to the overall field magnitude near the tip, the term linear in $z$ renders directly the near-tip $E_z$ value

$$(10)\qquad \varphi(r,z) \doteq \varphi(0,0) - zE_z(0,0) + O\left(r^2, z^2\right)$$

The expansion of Eq. (9) on substitution for $\rho$ from Eq. (6) and performing the integration after some tedious algebra (entrusted to Mathematica software), a lengthy expression for the field near the tip of the focal cone $E_z(0,0)$ is obtained. The leading terms giving the principle contribution are those that tend to grow infinitely for $z_1 \to 0$ and only these will be shown, with $z_1$ set equal to the caustic coordinate $z_c$. Using the same simplifying assumptions as in the case of the dipole calculation, namely that the temperature remains constant in the longitudinal direction $P_T = 1$ and the longitudinal density scale length is given by the cone length $z_n = z = z_b$, the result for the near-tip $z$-component of the electric field is

$$(11)\quad E_z \doteq -\frac{(k_B T_0)^{3/2}\tau_L}{e\sqrt{m_i} z_b}\frac{f}{R}\underbrace{\left[\log\left(\frac{R+\sqrt{R^2+f^2}}{R}\right)-\frac{R}{\sqrt{R^2+f^2}}\right]}_{2.78\times10^{-2}\ \text{for}\ R/f=0.3}\times\begin{cases}\dfrac{1}{r_c}\ \text{(exponential)}\\ \nu\left(\dfrac{2}{r_c}+\dfrac{\log(r_c f/Rr_b)}{r_b}\right)\ \text{(power }\nu\text{)}\end{cases}$$

for an exponential and power-ν dependence of the longitudinal density profile, respectively. The numerical value of the coefficient in the square brackets was evaluated to be equal to $2.78 \times 10^{-2}$ for the ration $R/f = 0.3$ as corresponding to the experiment [9]. The $z$-component of the electric field entering the cone tip is negative, pointing thus to a substantial negative charge accumulation near the tip and a deviation from the dipole field mentioned in the previous section. Again, as in the case of the magnetic field the field value $E_z$ diverges, too, when approaching the focus, the growth being halted by the finite size of the focal caustic.

## Evaluation of the fields for the spark in a model primordial atmosphere

The dipole electric field as well as the circulatory magnetic field generated near the cone surface will be evaluated for the condition of the experiment [9] using Eqs. (4) and (7), for the case of the exponential density profile dependence. The focused laser energy propagates down the tapering focal cone until the breakdown intensity is reached. Assuming the breakdown intensity for a CO-$N_2$ mixture 1:1 to be approximately equal to $10^{11}$ W·cm$^{-2}$ we obtain after some elementary calculations for the parameters of the focusing system used in the experiment (lens diameter 15 cm, focal length 25 cm, pulse energy 87 J, and pulse length 0.5 ns) the length of the spark (in front of the focus) about 2.5 cm, and its diameter on its broader end of about 1.5 cm. Setting as an example the temperature $T_0 = 500$ eV, from Eq. (4), the magnetic field near the plasma surface is obtained at the wider laser end of the spark $B \approx 27$ G. However, taking the standard Asterix laser beam divergence to be $5 \times 10^{-5}$ rad, the caustic diameter would be $2.5 \times 10^{-3}$ cm and the near tip value of $B$ would thus grow to about 16 kG. From Eq. (7), the expected value of the spark electric dipole moment $d_z \approx 3.2 \times 10^{-3}$ (in CGS units), the near tip value of the electric field intensity from Eq. (11) should amount to about $1.2 \times 10^2$ V/cm. Whether these calculated field values are sufficient to cause the observed imbalance between the optical isomers lies beyond the scope of this paper. The problem is addressed in a survey paper [10]. However, even there no quantitative estimates are mentioned. Since both the forms are not energetically different, it is to be expected that a relatively weak external field can cause an optical asymmetry.

## Conclusion

A fairly simple model of laser spark plasma formed by a delayed breakdown mechanism [7] within the focal cone of a focused ns laser beam in a gas at nearly atmospheric pressure implies quite convincingly that in a close vicinity of the spark plasma magnetic and electric fields are being spontaneously created. The magnetic field originates due to the standard mechanism of crossed density and temperature gradients, whereas the electric field is induced by a charge separation (polarization) of the plasma streaming radially across the self-generated magnetic field. Putting in the parameters of the experiment [9] performed at the PALS centre in Prague, values of the magnetic field intensity evaluated near the plasma tip may reach kG values and the accompanying electric field intensity lies in the range of 100 V/cm. Since the spark plasma is characterized by a rising density when going away from the focus (a difference from the more conventional laser experiments with a solid target, see [5]), the spark magnetic field winds round the optical axis in the opposite (anticlockwise) direction. The induced electric field examined at a larger distance from the spark (plasma cone) is pointing to the existence of an electric dipole oriented in the positive $z$-direction, i.e. with the positive charge facing the laser, in conformity with the experimental findings [6]. Since, obviously, the most intense radiation chemistry in the gas mixture is going on next to the focal caustic (cone tip), it is to be expected that the predicted presence of relatively strong ambient fields in this region will imprint itself on the chemical products in the form of racemization imbalance.

**Acknowledgment.** A support by the Czech Ministry of Education project MSMT COST no. LD14089 as well as the INGO II (CERN cooperation) project of the same ministry no. LG13031 are gratefully acknowledged.

This work was performed at the Institute of Physics ASCR in Prague, Czech Republic.

## References

1. Miller, S. L. (1953). A production of amino acids under possible primitive Earth conditions. *Science*, *117*, 528–529. DOI: 10.1126/science.117.3046.528.
2. Civiš, S., Babánková, D., Cihelka, J., Sazama, P., & Juha, L. (2008). Spectroscopic investigations of high-power laser-induced dielectric breakdown in gas mixtures containing carbon monoxide. *J. Phys. Chem.*, *112*, 7162–7169. DOI: 10.1021/jp712011t.
3. Juha, L., & Civiš, S. (2008). Laser-plasma chemistry. In M. Lackner (Ed.), *Chemical reactions initiated by laser-produced plasmas, lasers in chemistry*. (Vol. 2, (pp. 829–921). Weinheim: Wiley-VCH.
4. Ferus, M., Nesvorný, D., Sponer, J., Kubelík, P., Michalčíková, R., Shestivska, V., Sponer, J. E., & Civiš, S. (2015). High-energy chemistry of formamide: A unified mechanism of nucleobase formation. *Proc. Natl. Acad. Sci. U. S. A.*, *386*, 657–662. DOI: 10.1073/pnas.1412072111.

5. Managadze, G. (2007). A new universal mechanism of organic compounds synthesis during prebiotic evolution. *Planet Space Sci*., *55*, 134–140. DOI: 10.1016/j.pss.2006.05.024.
6. Zhivopistsev, E. S., Klimov, I. V., Markelov, E. Yu., Korobkin, V. V., & Motylev, S. L. (1992). Study of the electric field of a laser spark produced in a breakdown of the air. *Bull. Russ. Acad. Sci. Phys*., *56*, 1335–1341.
7. Raizer, Yu. P. (1974). *Lazernaya iskra i rasprostranenie razriadov*. Moskva: Izdatelstvo Nauka; see also Raizer, Yu. P. (1977). *Laser-induced discharge phenomena*. New York, London: Consultants Bureau.
8. Bessarab, A. V., Dalgaleva, G. V., Zhidkov, N. V., Kainov, V. Yu., Kormer, S. B., Pavlov, D. V., Urlin, V. D., Funtikov, A. I., & Yakutov, B. P. (1992). O raspade vozdushnoy plazmy obrazovannoy lazerom. In G. A. Kirillov, M. V. Sinitsyn, & V. D. Urlin (Eds.), *Veshchestvo v ekstremalnykh usloviyakh* (Trudy uchenykh yadernykh tsentrov Rossii, pp. 156–162). Nizhny Novgorod: MAE RF, RFYaTs-VNIIEF.
9. Civiš, S., Juha, L., Babánková, D., Cvačka, J., Frank, O., Jehlička, J., Králiková, B., Krása, J., Kubelík, P., Muck, A., Pfeifer, M., & Ullschmied, J. (2004). Amino acid formation induced by high-power laser in $CO_2$/CO-$N_2$-$H_2O$ gas mixtures. *Chem. Phys. Lett*., *386*, 169–173. DOI: 10.1016/j.cplett.2004.01.034.
10. Cintas, P., & Viedmon, C. (2012). The physical basis of asymmetry and homochirality. *Chirality*, *24*, 894–908. DOI: 10.1002/chir.